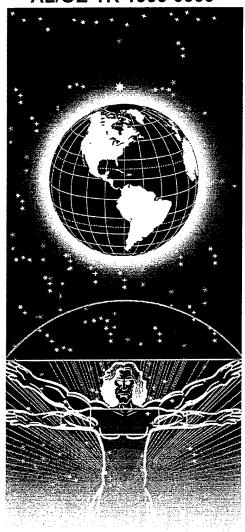AL/OE-TR-1995-0066

UNITED STATES AIR FORCE
ARMSTRONG LABORATORY

Comparison of Anatomical Characteristics of the Skin for Several Laboratory Animals

John H. Grabau
Lily Dong

GEO-CENTERS, Inc.
7 Wells Avenue
Newton Centre MA 02159

David R. Mattie
Gary W. Jepson
James N. McDougal

Toxicology Division, Occupational and
Environmental Health Directorate, Armstrong Laboratory
Wright-Patterson AFB OH 45433-7400

December 1995

19970604 171

TECHNICAL REVIEW AND APPROVAL

AL/OE-TR-1995-0066

The animals used in this study were handled in accordance with the principles stated in the *Guide for the Care and Use of Laboratory Animals*, Institute of Laboratory Animal Resources, National Research Council, National Academy Press, 1996, and the Animal Welfare Act of 1966, as amended.

This report has been reviewed by the Office of Public Affairs (PA) and is releasable to the National Technical Information Service (NTIS). At NTIS, it will be available to the general public, including foreign nations.

This technical report has been reviewed and is approved for publication.

FOR THE COMMANDER

TERRY A. CHILDRESS, Lt Col, USAF, BSC
Director, Toxicology Division
Armstrong Laboratory

REPORT DOCUMENTATION PAGE

Public reporting burden for this collection of information is estimated to average 1 hour per response, including the time for reviewing instructions, searching existing data sources, gathering and maintaining the data needed, and completing and reviewing the collection of information. Send comments regarding this burden estimate or any other aspect of this collection of information including suggestions for reducing this burden to Washington Headquarters Services, Directorate for Information Operations and Reports, 1215 Jefferson Davis Highway, Suite 1204, Arlington, VA 22202-4302, and to the Office of Management and Budget, Paperwork Reduction Project (0704-0188), Washington, DC 20503

1. AGENCY USE ONLY (Leave Blank)	2. REPORT DATE December 1995	3. REPORT TYPE AND DATES COVERED Interim - November 1993 - October 1994

4. TITLE AND SUBTITLE
Comparison of Anatomical Characteristics of the Skin for Several Laboratory Animals

5. FUNDING NUMBERS
Contract N00014-95-D-0048
PE 61102F
PR 2312
TA 2312A2
WU 2312A201

6. AUTHOR(S)
John H. Grabau, Lily Dong, David R. Mattie, Gary W. Jepson and James N. McDougal

7. PERFORMING ORGANIZATION NAME(S) AND ADDRESS(ES)
GEO-CENTERS, Inc.
7 Wells Avenue
Newton Centre MA 02159

8. PERFORMING ORGANIZATION REPORT NUMBER

9. SPONSORING/MONITORING AGENCY NAME(S) AND ADDRESS(ES)
Armstrong Laboratory, Occupational and Environmental Health Directorate
Toxicology Division, Human Systems Center
Air Force Materiel Command
Wright-Patterson AFB OH 45433-7400

10. SPONSORING/MONITORING AGENCY REPORT NUMBER
AL/OE-TR-1995-0066

11. SUPPLEMENTARY NOTES

12a. DISTRIBUTION/AVAILABILITY STATEMENT
Approved for public release; distribution is unlimited.

12b. DISTRIBUTION CODE

13. ABSTRACT (Maximum 200 words)

Anatomical differences between experimental species may affect the relative rates of chemical penetration into and through the skin. Computer-based morphometric techniques were used to quantitate selected morphologic characteristics within the epidermal and dermal regions of dorsal midline skin of the Hartley and IAF (Hairless) Guinea pigs, $B_6C_3F_1$ and SKH1 (Hairless) mice, Fuzzy and Fischer (F-344) rats, mixed breed farm pigs and Rhesus monkeys. The cutaneous thickness measurements included the stratum corneum, the stratum germinativum, the underlying viable epidermis and the dermis. Vascular measurements included the average depth and fractional area for capillaries, venules and arterioles. Adnexal measurements included the average depth and fractional area of hair follicles and sebaceous glands and the average number of follicular ostia per unit surface area. Statistical analysis revealed comparative differences that could not be attributable to animal size. These measurements will allow for an improved understanding of the anatomical differences of skin in laboratory animals. This understanding is critical to facilitate extrapolation of chemical absorption in animals to humans.

14. SUBJECT TERMS

Chemical penetration	Dermal	Epidermal	Rats
Guinea pigs	Mice	Pigs	Monkeys

15. NUMBER OF PAGES
38

16. PRICE CODE

17. SECURITY CLASSIFICATION OF REPORT UNCLASSIFIED	18. SECURITY CLASSIFICATION OF THIS PAGE UNCLASSIFIED	19. SECURITY CLASSIFICATION OF ABSTRACT UNCLASSIFIED	20. LIMITATION OF ABSTRACT UNLIMITED

THIS PAGE INTENTIONALLY LEFT BLANK

TABLE OF CONTENTS

LIST OF TABLES

PREFACE

Anatomical differences between experimental species may affect the relative rates of chemical penetration into and through the skin. Computer-based morphometric techniques were used to quantitate selected morphologic characteristics within the epidermal and dermal regions of dorsal midline skin of the Hartley and IAF (Hairless) Guinea pigs, $B_6C_3F_1$ and SKH1 (Hairless) mice, Fuzzy and Fischer (F-344) rats, mixed breed farm pigs and Rhesus monkeys. The cutaneous thickness measurements included the stratum corneum, the stratum germinativum, the underlying viable epidermis and the dermis. Vascular measurements included the average depth and fractional area for capillaries, venules and arterioles. Adnexal measurements included the average depth and fractional area of hair follicles and sebaceous glands and the average number of follicular ostia per unit surface area. Statistical analysis revealed comparative differences that could not be attributable to animal size. These measurements will allow for an improved understanding of the anatomical differences of skin in laboratory animals. This understanding is critical to facilitate extrapolation of chemical absorption in animals to humans.

THIS PAGE INTENTIONALLY LEFT BLANK

INTRODUCTION

The cutaneous (skin) system is the largest organ system in both man and animals (1) and serves as a barrier to the exterior environment with important sensory and thermo-regulatory functions. Although the skin primarily functions as a barrier, it is an incomplete barrier that can allow chemical substances into the body. In toxicology, transdermal absorption can be a primary route of exposure for liquids or a secondary route of exposure for vapors. Adequately predicting the risk from occupational or accidental skin exposure to liquids and vapors requires a full understanding of the chemical absorption process.

A significant failing of toxicology research is the marginal ability of data from dermal absorption research in laboratory animals to be predictive of human exposures. This can be attributed to the currently-limited understanding of basic cutaneous physiology and comparative anatomical differences. There is often significant anatomical variation of skin between species and within individuals of the same species. Age, sex, location on the body, nutrition and hormonal status can affect not only the anatomical characteristics of skin, but also the metabolic and physiologic properties.

Reviews of dermatotoxicity, including that of All and Oehme(1992)(2), tend to concentrate on human or domestic animal anatomy and not that of common laboratory animals. A study conducted by Montereiro-Riveire, et al (1990) [3] is the only other investigation known to the authors in which anatomical features were measured in a number of species (i.e. the cat, cow, dog, horse, pig, rat, mouse, rabbit and monkey). In that study the thickness of the stratum corneum and epidermis and the number of cell layers at five various body sites were measured using an ocular micrometer.

The understanding of species differences in barrier function can be significantly improved by morphometrically defining the anatomical characteristics and differences between commonly studied laboratory animals and man. The most important components of skin which can affect the transport of compounds into the body are within three anatomical regions: (1) the epidermis, (2) the dermis, and (3) the subcutis or hypodermis. These regions and the dermo-epidermal junction have special structural and physiological properties as do the cutaneous adnexal components, nerves and vasculature.

Morphometry is the measurement of form and implies a sort of quantitative assessment of a form, such as length or area. Stereology, a subordinate field of morphometry, allows calculation of three dimensional quantitative parameters from measurements made on two dimensional images of three dimensional objects. Prior to the use of computers, images that were measured were often photographs or scale drawings of the form or object. Computer technology has allowed the original form or object to be viewed by a television camera and converted from an analog to a digital image. The digital image is well-suited for mathematical morphology including binary, grey and color image processing and measurement.

The objective of this investigation was to use computer-based morphometric techniques to quantitate selected morphologic characteristics within the epidermal and dermal regions in eight laboratory species.

STRUCTURE AND PHYSIOLOGY OF SKIN

The integumentary system is derived from a simple embryonic structure that becomes complex, matures and atrophies with age. It has two embryonic origins: a superficial layer called the epidermis, which develops from ectoderm; and a second, deep layer called the dermis, which develops from mesoderm. Initially, the epidermis is a single layer, but as the embryo matures, multiple layers are formed. Hairs are developed from epidermal invaginations into the dermis, and the surrounding dermal root sheath is formed by the dermal mesenchyme.

The epidermis is the outer skin and functions as a barrier to physical and chemical agents. This is primarily attributable to the properties of an epidermal cell product called keratin. Keratin is a filamentous protein that is insoluble and physically tough. This protein progressively accumulates in epidermal cells as they differentiate from basal cells, migrate toward the surface and eventually form a solid, protective thin envelope overlying the epidermis.

The epidermal cell types are keratinocytes, melanocytes, Langerhans cells and Merkel cells. The predominant cell type is the keratinocyte, and it occurs in three anatomical or morphological stages: (1) growth and proliferation (stratum germinativum/basal cell layer); (2) maturation and outward displacement (stratum spinosum/spinous cell layer and stratum granulosum/granular cell layer); and (3) dyshesion/desquamation (stratum corneum/cornified layer). These stages have distinct characteristics and appearances.

The epidermis can also be classified as: (1) the viable epidermis, which contains living, nucleated cells; and (2) the nonviable epidermis, a non-nucleated layer composed of end-stage cornified keratinocytes. The viable epidermis is composed of the basal cell layer, the spinous cell layer and the granular cell layer. The basal cell layer is mitotically active and has cuboidal cells that contain some keratin. The basal cell layer is the source of the keratinocytes which migrate away from the basement membrane and become transformed in the keratinocyte stages. The spinous cell layer contains more keratin and has larger elongated or flattened keratinocytes with increased cytoplasm.

The granular layer keratinocyte contains non-membrane bound granules measuring 1-5 microns in diameter. These granules are of two types: (1) a dense homogenous deposited (DHD) granule, and (2) a larger and more irregular granule, termed a keratohyalin granule. A transition occurs in the uppermost part of this layer. Cytoplasmic organelles, including the nuclei and filaments, are loosened. Keratohyalin granules disappear and are replaced by 7 to 8nm electron lucent filaments. The cell membrane is altered so that it is not solubilized by reducing or dissociating agents and can be hydrolyzed only by proteases. The upper spinous layer and granular layer also contain 2 to 3.5nm lamellar granules which are produced by golgi. These structures are secreted from the cells and deposited between keratinocytes. The epidermis is permeable to water at both the deepest and most superficial portions but is generally regarded as impermeable to water from either direction at the level of the granular layer.

The nonviable epidermis, termed the non-nucleated stratum corneum, represents the last stage of keratinization. The stratum corneum is composed predominately of keratin and is generally regarded as an impermeable sheet or layer to many compounds. In this stage of maturation, there is desquamation of keratinocytes. The histologic appearance of multiple-stacked thin keratin layers is related to continuous growth of the epidermis and waves of desquamation. The mechanism of keratinocyte dyshesion is debated and uncertain.

The dermal-epidermal junction anchors and supports the epidermis to the dermis and also serves as a barrier to certain large molecular compounds. It is composed of a basement membrane, which is a dense lamina of interwoven type IV collagen chains, and an underlying thin zone of anchoring filaments and microfibril bundles known as reticular fibers or reticulin

(type III collagen). The dense upper zone provides a surface for the epidermal cells to grow upon and is a medium that allows the transfer of nutritional and hormonal compounds. The thin underlying zone serves to attach overlying structures to the adjacent type I collagen fibers of the dermis.

The dermis provides flexible support to the skin by allowing stretching and also contains structures for thermo-regulation. It is extremely collagen-rich and contains nerves, vessels and the adnexa. The dermis can be divided into the superficial and reticular dermis. The superficial dermis, or papillary dermis, is a loosely-packed fibrous tissue composed of collagen fibers, thick and thin elastic fibers, and ground substance. Ground substance is a gel of hydrophilic, amorphous material that forms a matrix that embeds extracellular fibers. It is composed of amino(proteo)glycans and glycosaminoglycans (hyaluronic acid, chondroitin sulfate, dermatan sulfate). The reticular dermis is composed predominantly of densely-packed, thick fibrous collagen bundles.

The skin is the largest sensory organ of the body. The dermal nerves are branches of spinal and trigeminal nerves. The afferent sensory cutaneous nerves sense pressure, pain, heat and cold. The efferent cutaneous nerves innervate vessels and help regulate cutaneous blood flow. Blood flow in capillaries is not solely regulated by innervation. The mediators of inflammation, such as vasoactive amines, plasma kinins and prostaglandins, are well recognized to influence blood flow by affecting vascular permeability.

Blood vessels have a role of metabolic supply and thermal regulation. Not all capillaries in the dermis are distributed randomly. Many are grouped in a layered fashion known as a dermal plexus. In humans, the superficial, intermediate and deep dermal plexuses are recognized. There are scant references to dermal plexus in animals. The plexuses also surround adnexal structures as they invaginate into the dermis in a glove-like fashion.

The anatomical link between the arteriole and the venule is most often the capillary but can be a glomus body, a structure for shunting blood. Arterio-venous shunts, through glomus bodies, occur in regions of nail beds (finger and toe nails; claws, hooves) and also in the lips and nose. Lymphatics are also present in the dermis and tend to follow the same pathways as blood vessels. Their morphologic features include distended lumens, thin walls and prominent valves.

The adnexa are cutaneous appendages and may include hair, sebaceous glands and sweat glands. There is significant variation between species in the composition and distribution of the adnexa. Hair is a keratinized structure produced in a hair follicle. The free portion of the hair above the skin is the hair shaft. The hair root, which terminates as the hair bulb at the dermal papilla, is inside the follicle. The hair is composed of a cortex of densely-compact keratinized cells and a medulla of loosely-filled cuboidal or flattened cells.

Hair follicles are composed of an inner root sheath adjacent to the hair and an outer root sheath. The dermal papillae are composed of the hair matrix cells, which are similar to epidermal basal cells. Hair follicles can occur as primary or secondary follicles and can be single or compound. Primary follicles have roots that extend deeply into the dermis and are often associated with sebaceous glands or sweat glands. Secondary follicles have roots closer to the surface and are of a smaller diameter. They may have associated sebaceous glands but not sweat glands. A single or simple follicle has only one hair emerging, while a compound follicle may have several. The distribution of emerging hair follicles varies widely between species.

Sweat glands are morphologically classified as apocrine type and merocrine (eccrine) type. Apocrine glands are simple tubular glands and are the most developed type in animals; however, the incidence in animal species varies widely. Merocrine glands are found mainly in

foot pads and nasolabial regions. Sebaceous glands can be simple, compound or branched holocrine glands that originate from the external root sheath. They are often associated with hair follicles into which they release sebum.

The remaining subcutis layer is fibro-fatty tissue that insulates and cushions the body. It is composed of adipose tissue, collagen and muscle.

MATERIALS AND METHODS

Laboratory Animals

Cutaneous specimens were obtained from ten individual animals of the following three rodent species (six strains): Hartley Guinea pig, IAF (Hairless) Guinea pig, $B_6C_3F_1$ mice, SKH1 (Hairless) mice, Fuzzy rats and Fischer 344 (F-344) rats. The Hartley Guinea pigs (or Crl:(HA)BR) are an outbred strain. The IAF Hairless Guinea pigs (or Crl:IAF/HA(hr/hr)BR) are mutants derived from Hartley Guinea pigs. The $B_6C_3F_1$ mice (or $B_6C_3F_1$/CrlBR) are hybrid mice derived from a cross between female $C_{57}BL$/6NCrlBR and male C_3H/NeNCrlBR mice. The SKH1 (Hairless) mice (or Crl:SKH1()hr/hrBR) are an outbred non-pedigreed/uncharacterized hairless strain of mice. The Fuzzy rat (or WF/PmWp-"fz") is a hypotrichotic mutant derived from inbred Wistar Furth (WF) rats. The Fischer rats (or CDF (F-344)/CrlBR) are inbred rats. Additionally, specimens were obtained from five mixed breed farm pigs and five Rhesus monkeys.

Animals were male with the exception of the farm pigs. Rodents, approximately 90 days old, were obtained from Charles River Laboratories (Wilmington MA), with the exception of the Fuzzy rats which were obtained from a colony maintained at Armstrong Laboratory, Comparative Medicine Branch, Wright-Patterson AFB, OH. The Rhesus cutaneous biopsies were obtained from animals in a colony at Wright-Patterson AFB and were approximately 10-12 years old. The mixed breed farm pigs were obtained from a local source and were approximately 3 months old.

Animal weights were within the following ranges:

Hartley Guinea pig	600-700 grams
Hairless Guinea pig	600-700 grams
$B_6C_3F_1$ mice	28 - 32 grams
SKH1 Hairless mice	28 - 34 grams
Fuzzy rats	300-325 grams
Fischer 344 (F-344) rats	225-250 grams
Mixed breed farm pigs	70 - 80 lbs/35 Kg
Rhesus monkeys	10 - 12 Kg

Sample Preparation

Cutaneous specimens were taken from the dorsal mid-line in the mid-thoracic region. Specimens were fixed in buffered formalin and embedded in paraffin. Four micron tissue sections were cut in a routine histologic manner (perpendicular to the epidermal surface) and stained with hematoxylin and eosin (H&E) or Masson's trichrome stain. A second tissue specimen was obtained from each rodent species and fixed in buffered formalin; however, the specimen, when embedded in paraffin, was aligned to allow sectioning in a plane parallel to the surface. It was sectioned at a depth of the dermal-epidermal junction and stained with H&E.

Morphometric Analysis

All measurements were performed on routine histologic specimens, except for those associated with hair follicle counts per cutaneous surface area which were obtained from the second histologic section.

Quantitative image analysis was performed using a Quantimet 570c Image Analysis System (Leica, Inc., Deerfield, IL.). The Quantimet 570c Image Analysis system is composed of

a microscope with a mounted 3CCD color camera, an analysis system and a controlling computer. The analysis system is composed of a video preprocessor, a morphological processor, a measurement processor and a video postprocessor. The controlling computer conducts the various analysis processors through an interfacing 68000 Motorola processor.

A - Hair
B - Stratum Corneum
C - Stratum Granulosum and Viable Epidermis
D - Basement Membrane
E - Sebaceous Gland
F - Hair Follicle
G - Vessles

These principles were used to define areas for image analysis:

1. Epidermal thickness measurements were conducted in inter-follicular regions and excluded epithelia associated with hair follicles. A single epidermal thickness measurement was the distance between the uppermost portion of the attached stratum corneum to the lowest portion of the viable epidermis along a single chord (see Appendix A).

2. Measurements of depth were based in relationship to the basement membrane at the dermal-epidermal junction. At points where hair follicles were visible as directly confluent with inter-follicular ep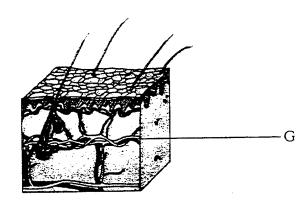ithelia, the measurement was based on the artificial creation of a line to represent the basement membrane. This line extended from the inter-follicular basement membrane, across the follicle and rejoined with the opposite inter-follicular basement membrane.

3. Depth measurements for vessels and adnexa were from the basement membrane to the center of the feature measured.

Epidermal measurements were conducted with a 40x objective at three random inter-follicular sites from a routine H&E stained histologic section. The computer-based image analysis algorithm allowed for multiple serial measurements of epidermal region thicknesses at 10 pixel intervals. The measured epidermal regions were the stratum corneum, stratum granulosum and underlying viable epidermis. Follicular counts per surface area were taken with a 20x objective using the special sectioning described above.

Dermal vascular measurements were conducted with the 40x objective and included the number, center depth from the basement membrane and cross sectional area of capillaries, arterioles and venules. The computer-based algorithm used for these measurements allowed for mapping of the tissue at a low magnification into grids or regions and subsequent measurement of the grid or region at the higher magnification. A similar mapping algorithm was used for adnexal measurement using a 20x objective for quantitative analysis. Adnexal measurements included the number, center depth and cross-sectional area of hair follicles and glands of the analyzed tissue.

A detailed description of the algorithms mentioned is present in Appendix A.

Statistical Analysis

Measurements made by the Quantimet 570c Image Analysis System were saved in ASCII computer file format. These ASCII files were imported into RS/1 (BBN Software Products Corp., Cambridge MA) and formatted for statistical analysis by BMDP 1D and 7D (BMDP Statistical Software, Inc., Los Angeles, CA). Manually counted and tabulated follicular ostia data were manually entered into RS/1. Averages and standard deviations were first made of data from individual animal measurements. Individual animal measurement averages of a species were then compiled to determine species averages and standard deviations (Tables 1a, 2a, 3a, 4a, 5a). One factorial analysis of variance with Bonferroni multiple comparison was conducted on species averages to determine which species measurements were significantly different ($p < .05$)(Tables 1b, 2b, 3b, 4b, 5b).

RESULTS

The Hairless Guinea pig (Tables 1a and 1b) had the thickest total epidermis as well as the thickest stratum corneum, stratum granulosum and viable epidermis. The $B_6C_3F_1$ mouse had the thinnest total epidermis and the thinnest viable epidermis. The $B_6C_3F_1$ mouse and the F-344 rats had the thinnest stratum granulosum. The strains with the thickest layers were about six times thicker than the strains with the thinnest layers.

The shortest average vascular depth for capillaries, venules and arterioles (Tables 2a and 2b) was present in the two mouse strains, the $B_6C_3F_1$ mice and the SKH1 Hairless mice. The greatest average depth for capillaries and arterioles was found in the F-344 rat and the Fuzzy rat. The Rhesus monkey had the greatest average venule depth. The depth of the blood vessels varied two-fold between the strains.

Analysis of the fractional area (Tables 2a and 2b) of dermal blood vessels resulted in few groups with significant differences. The fractional area of dermal capillaries, arterioles and venules was greatest in the SKH1 mouse. The capillary fractional area was not significantly different between the Rhesus monkey, the F-344 rat, the Fuzzy rat, the pig, the Hartley Guinea pig and the Hairless Guinea pig. The venule fractional area was not statistically different between any of the species. The arteriole fractional area was least in the Hairless Guinea pig, the Fuzzy rat, the $B_6C_3F_1$ mice and the Hartley Guinea pig. Capillary fractional area varied by a factor of two between statistically different strains, while the arteriole fractional area varied over a factor of five and venule fractional area varied by a factor of nine.

The greatest average follicular and sebaceous gland depth as well as fractional area (Tables 3a and 3b) were found in the pig. Follicles in the pig were approximately seven times deeper than in the $B_6C_3F_1$ mouse, which had the least depth. Sebaceous glands in the pig were about eleven times deeper than those of the mouse. The smallest follicular fractional area was present in the F-344 rat, and the smallest sebaceous gland fractional area was found in the Hartley Guinea pig. Follicular and sebaceous gland fractional area varied up to ten-fold between strains.

The number of follicular ostia per unit surface area (Tables 4a and 4b) was highest in the $B_6C_3F_1$ mouse and was lowest in the pig. The number of follicular ostia in the $B_6C_3F_1$ mice was about four times greater than those of the pig. Due to the presumed loss of some sectioned hairs within ostia, it was not possible to correlate ostia to hairs within ostia.

The thickness of the dermis (Tables 5a and 5b) was greatest in the pig and the least in the mouse strains with approximately an eight-fold difference in thickness between these species.

Table 1a. Thickness of Epidermal Components in Eight Laboratory Species in Microns
Ten animals were sampled in each strain (10 samples) except for five primates (5 samples) and the five pigs (5 samples), each sample was measured at three different inter-follicular sites.

		SKH1 mouse	$B_6C_3F_1$ mouse	Hartley guinea pig	Hairless guinea pig	Fuzzy rat	F-344 rat	Pig	Rhesus monkey
Stratum corneum	MEAN	10.0	6.2	29.3	35.9	23.2	11.2	21.9	4.2
	SD	2.6	2.9	9.3	9.7	5.4	5.1	9.0	1.5
Stratum granulosum	MEAN	6.6	3.2	8.5	19.4	10.5	3.0	4.9	4.8
	SD	1.8	1.3	2.1	4.7	2.5	0.4	2.0	1.0
Viable epidermis	MEAN	30.1	11.9	24.7	60.1	52.2	18.3	52.7	26.8
	SD	10.0	4.2	3.4	9.4	10.0	6.3	12.9	3.2
Total epidermis	MEAN	46.7	21.3	62.6	115.4	86.0	32.6	79.5	35.7
	SD	10.2	6.1	13.7	17.1	13.3	7.3	14.1	3.6

9

Table 1b. Significant Differences in the Thickness of Epidermal Components
Species which are not significantly different (p < .05)are grouped by a connecting line.
The mean in micros is below each strain.

Stratum corneum

Hairless guinea pig	Hartley guinea pig	Fuzzy rat	Pig	F-344 rat	SKH1 mouse	$B_6C_3F_1$ mouse	Rhesus monkey
35.9	29.3	23.2	21.9	11.2	10.0	6.2	4.2

Stratum granulosum

Hairless guinea pig	Fuzzy rat	Hartley guinea pig	SKH1 mouse	Pig	Rhesus monkey	$B_6C_3F_1$ mouse	F-344 rat
19.4	10.5	8.5	6.6	4.9	4.8	3.2	3.0

Viable epidermis

Hairless guinea pig	Pig	Fuzzy rat	SKH1 mouse	Rhesus monkey	Hartley guinea pig	F-344 rat	$B_6C_3F_1$ mouse
60.1	52.7	52.2	30.1	26.8	24.7	18.3	11.9

Total epidermis

Hairless guinea pig	Fuzzy rat	Pig	Hartley guinea pig	SKH1 mouse	Rhesus monkey	F-344 rat	$B_6C_3F_1$ mouse
115.4	86.0	79.5	62.6	46.7	35.7	32.6	21.3

Table 2a. Depth[1] and Fractional Area[2] of Dermal Blood Vessels

Ten animals were sampled in each strain (10 samples) except for five primates (5 samples) and the five pigs (5 samples).

	SKH1 mouse	B6C3F1 mouse	Hartley guinea pig	Hairless guinea pig	Fuzzy rat	F-344 rat	Pig	Rhesus monkey
Capillary depth (microns)								
NUMBER	289	142	403	453	336	296	276	97
MEAN	287.7	276.6	433.2	356.0	520.1	560.9	401.3	495.2
SD	71.3	122.7	156.5	45.5	146.4	195.6	114.7	89.4
Capillary fractional area								
MEAN	0.7	0.7	0.3	0.3	0.3	0.3	0.3	0.4
SD	0.4	0.6	0.1	0.1	0.03	0.1	0.2	0.1
Venule depth (microns)								
NUMBER	48	16	44	63	25	29	14	6
MEAN	434.3	402.9	563.3	514.6	723.8	798.8	701.0	916.6
SD	106.9	150.7	255.0	189.8	218.9	285.7	198.5	182.9
Venule fractional area (cm^2/m^2)								
MEAN	5.3	2.7	2.1	0.9	1.2	3.6	4.5	0.7
SD	4.1	1.6	1.4	0.2	0.6	8.7	3.1	0.2
Arteriole depth (microns)								
NUMBER	18	3	47	68	18	43	17	13
MEAN	424.3	467.0	536.6	543.8	79.4	902.3	710.7	468.9
SD	125.3	147.4	256.0	209.2	288.5	289.3	237.3	219.4
Arteriole fractional area								
MEAN	2.3	0.7	0.9	0.6	0.6	1.3	1.1	1.2
SD	2.0	0.2	0.5	0.3	0.2	0.9	1.2	0.5

(1) Depth in micros is measured from the geometric center of the visible vessel cross-sectional area to the basement membrane.

(2) Fractional Area equals a ratio of the sum of the cross-sectional area of a category (such as capillaries) to the total dermal tissue area measured. Area measurements are in square microns (μ^2)

Table 2b. Significant Differences in the Depth[1] and Fractional Area[2] of Dermal Blood Vessels

Species which are not significantly different (p <.05) are grouped by a connecting line. The mean is below each strain.

Capillary depth (microns)

F-344 rat	Fuzzy rat	Rhesus monkey	Hartley guinea pig	Pig	Hairless guinea pig	SKH1 mouse	B₆C₃F₁ mouse
560.9	520.1	495.2	433.2	401.3	356.0	287.7	276.6

Capillary fractional area (cm²/m²)

SKH1 mouse	B₆C₃F₁ mouse	Rhesus monkey	Hartley guinea pig	Pig	Hairless guinea pig	Fuzzy rat	F-344 rat
0.7	0.7	0.4	0.3	0.3	0.3	0.3	0.3

Venule depth (microns)

Rhesus monkey	F-344 rat	Fuzzy rat	Pig	guinea pig	Hartley guinea pig	Hairless SKH1 mouse	B₆C₃F₁ mouse
916.6	798.8	723.8	701.0	563.3	514.6	434.3	402.9

Venule fractional area (cm²/m²)

SKH1 mouse	Pig	F-344 rat	B₆C₃F₁ mouse	Hartley guinea pig	Fuzzy rat	Hairless guinea pig	Rhesus monkey
5.3	4.5	3.6	2.7	2.1	1.2	0.9	0.7

Arteriole depth (microns)

F-344 rat	Fuzzy rat	Pig	guinea pig	Hairless guinea pig	Hartley Rhesus monkey	B₆C₃F₁ mouse	SKH1 mouse
916.6	798.8	723.8	701.0	563.3	514.6	434.3	434.3

Arteriole fractional area (cm²/m²)

SKH1 mouse	F-344 rat	Rhesus monkey	Pig	Hartley guinea pig	B₆C₃F₁ mouse	Hairless guinea pig	Fuzzy monkey
902.3	793.4	710.7	543.8	536.6	468.9	467.0	424.3

(1) Depth in micros is measured from the geometric center of the visible vessel cross-sectional area to the basement membrane.
(2) Fractional Area equals a ratio of the sum of the cross-sectional area of a category (such as capillaries) to the total dermal tissue area measured. Area measurements are in square microns (μ^2)

Table 3a. Depth[1] and Fractional Area[2] of Dermal Adnexa
Ten animals were sampled in each strain (10 samples) except for five primates (5 samples) and the five pigs (5 samples).

	SKH1 mouse	$B_6C_3F_1$ mouse	Hartley guinea pig	Hairless guinea pig	Fuzzy rat	F-344 rat	Pig	Rhesus monkey
Follicle depth (microns)								
NUMBER	173	328	385	397	177	3664	19	43
MEAN	364.9	183.3	504.0	433.9	566.2	388.4	1330.6	840.3
SD	117.6	56.0	155.6	95.8	103.3	102.4	510.4	216.9
Follicle fractional area								
MEAN	21.0	7.8	18.9	25.6	19.0	5.9	63.6	49.9
SD	5.7	5.8	10.4	3.5	8.7	3.7	43.9	20.6
Gland depth (microns)								
NUMBER	157	181	126	286	103	128	5	22
MEAN	230.6	4160.0	351.1	327.6	402.6	411.6	1771.0	771.5
SD	89.4	35.6	178.7	121.9	50.2	72.2	646.8	62.1
Gland fractional area								
MEAN	18.2	6.9	4.6	10.4	30.9	7.4	50.5	22.2
SD	10.7	4.9	2.6	2.0	9.2	3.4	49.6	12.6

(1) Depth in microns is measured from the geometric center of the visible follicle or sebaceous gland cross-sectional area to the basement membrane.
(2) Fractional Area equals a ratio of the sum of the cross-sectional area of a category (such as follicles) to the total dermal tissue area measured. Area measurements are in square mincrons (μ^2).

Table 3b. Significant Differences in Depth[1] and Fractional Area[2] of Dermal Adnexa

Species which are not significantly different (p <.05)are grouped by a connecting line.

Follicle depth (microns)

Pig	Rhesus monkey	Fuzzy rat	Hartley guinea pig	Hairless guinea pig	F-344 mouse	SKH1 mouse	$B_6C_3F_1$ mouse
1330.6	840.3	566.2	504.0	433.9	388.4	364.9	183.3

Follicle Fractional Area (cm²/m²)

Pig	Rhesus monkey	Hairless guinea pig	SKH1 mouse	Fuzzy rat	Hartley guinea pig	$B_6C_3F_1$ mouse	F-344 rat
63.6	49.9	25.6	21.0	19.0	18.9	7.8	5.9

Sebaceous Gland Depth (microns)

Pig	Rhesus monkey	F-344 rat	Fuzzy rat	Hartley guinea pig	Hairless guinea pig	SKH1 mouse	$B_6C_3F_1$ mouse
1771.0	771.5	411.6	402.6	351.1	327.6	230.6	160.0

Sebaceous Gland Fractional Area (cm²/m²)

Pig	Fuzzy rat	Rhesus monkey	SKH1 mouse	Hairless guinea pig	F-344 rat	$B_6C_3F_1$ mouse	Hartley guinea pig
50.5	30.9	22.2	18.2	10.4	7.4	6.9	4.6

(1) Depth in microns is measured from the geometric center of the visible follicle or sebaceous gland cross-sectional area to the basement membrane.

(2) Fractional Area equals a ratio of the sum of the cross-sectional area of a category (such as follicles) to the total dermal tissue area measured. Area measurements are in square mincrons (μ^2).

14

Table 4a. Number of Follicular Ostia per Square Millimeter

Five animals were sampled in each strain (5 samples).

	SKH1 mouse	$B_6C_3F_1$ mouse	Hartley guinea pig	Hairless guinea pig	Fuzzy rat	F-344 rat	Pig	Rhesus monkey
MEAN	7.9	38.4	15.4	19.3	14.2	21.9	0.9	5.6
SD	2.2	5.1	1.8	0.8	1.4	5.1	0.3	1.1

Table 4b. Significant Differences of Follicular Ostia Number

Species which are not significantly different (p <.05) are grouped by a connecting line. The mean of the number of follicular ostia per square millimeter is below each strain.

$B_6C_3F_1$ mouse	F-344 rat	Hairless guinea pig	Hartley guinea pig	Fuzzy rat	SKH1 mouse	Rhesus monkey	Pig
38.4	21.9	19.3	15.4	14.2	7.9	5.6	0.9

15

Table 5a. Dermal Thickness in Microns
Five animals were sampled in each strain (5 samples).

	SKH1 mouse	$B_6C_3F_1$ mouse	Hartley guinea pig	Hairless guinea pig	Fuzzy rat	F-344 rat	Pig	Rhesus monkey
MEAN	428.2	497.8	2354.6	1616.0	1108.2	1105.4	3848.2	1457.2
SD	91.2	89.2	322.0	189.9	123.9	71.2	1017.7	167.5

Table 5b. Significant Differences in Dermal Thickness in Microns
Species which are not significantly different (p <.05) are grouped by a connecting line. The mean is below each strain.

Pig	Hartley guinea pig	Hairless guinea pig	Rhesus monkey	Fuzzy rat	F-344 rat	$B_6C_3F_1$ mouse	SKH1 mouse
3848.2	2354.6	1616.0	1457.2	1108.2	1105.4	497.8	428.2

DISCUSSION

The objective of this investigation was to quantitate selected morphologic characteristics within the epidermal and dermal regions in eight laboratory species. The measurements will allow for an improved understanding of the anatomical differences of skin in laboratory animals. This understanding is critical to facilitate extrapolation of chemical absorption in animals to humans.

A search for literature containing a quantitative comparison of skin from laboratory animals produced only one article by Monteiro-Riviere, et al[3]. The cat, cow, dog, horse, pig (Yorkshire), rat (Sprague-Dawley), mouse (BLB/cByS), rabbit and monkey (Macaca mulata) were studied in that investigation. While the present study used several similar species (mice, rats, pigs and monkeys), only the Macaca mulata was identical. Comparison of paraffin embedded skin epidermal thickness data (Table 6) from Monteiro-Riviere, et al (1990)[3] with data obtained from this investigation (stratum corneum and viable epidermis) revealed a similarity between the haired strains. However our comparison between the two investigations of stratum corneum thickness showed approximately a two-fold greater thickness in our study for the rat, mouse and pig, yet a three-fold reduction in thickness for the rhesus monkey. It is uncertain if this is due solely to a true difference between the samples or the methods by which the stratum corneum was measured. There are three potentially significant differences in the methods of measurement. The first difference is that Monteiro-Riviere, et al (1990)[3] used a calibrated ocular micrometer, while this investigation measured digitized images. This is significant because the digitized image obtained with the 40x objective can be resolved with an accuracy of 0.66 micron. Also, and perhaps more importantly, a digitized image can contain up to 256 shades of grey when converted to a grey scale or monochrome image. All of these shades can be resolved digitally, while the human eye can only resolve 25 to 50 shades. This greatly aides recognition of image edges in the loosely attached stratum corneum. The second difference is that the stratum corneum measured in this investigation included the loose, non-compact superficial layers with its thickness corrected to subtract the space between the layers, while Monteiro-Riviere, et al (1990)[3] measured only the compact stratum corneum. The third difference is that the previous investigation made three measurements per image, while this investigation made approximately 50 to 60 measurements per image. An additional factor that may have specifically affected the rhesus monkey stratum corneum thickness in this study could have been the surgical preparation of the biopsy site and use of topical disinfectants prior to the cutaneous biopsy. This may have removed a portion of the stratum corneum.

Table 6. Montereiro-Riveire, *et al*[5] Measurements of Paraffin Sectioned Thoraco-lumbar Skin

	BLB/cByS mouse	Sprague-Dawley rat	Yorkshire pig	Rhesus monkey
Stratum corneum thickness (microns)	2.9000 ± 0.12	5.0 ± 0.85	12.28 ± 0.72	12.05 ± 2.30
Epidermal thickness[1] (microns)	13.32 ± 1.19	21 ± 2.23	51.89 ± 1.49	26.87 ± 3.41

[1] Epidermal thickness in the Monteiro-Riviere, *et al*[3] investigation equals the sum of the stratum granulosum thickness and viable epidermis thickness in this investigation.

Two factors may have affected the accuracy of the measurements. The first involved the reliability of stratum corneum thickness measurements from processed tissues to represent the thickness present on the intact animal. Due to the nature of the stratum corneum, it can only be assumed that the most superficial portions are likely to be separate from the deeper portions during tissue processing. While all tissues were treated identically to avoid variation, it is unknown if the assumed loss is identical or even proportional between species.

The second factor involved the effect of tissue shrinkage. The fixation of tissue by buffered formalin is generally believed to induce tissue shrinkage. The degree of shrinkage in the cutaneous tissues examined is unknown. Because of the probability of this tissue change, the measurements and comparisons made between species should be considered relative comparisons, and values should not be considered absolute. The future determination of a shrinkage factor coefficient could allow for conversion of some measurements to represent their actual values in the intact animal more closely.

Blood flow is a dynamic event in any organ of the intact animal, especially the skin. The detection and measurement of vascular channels do not allow for the prediction or determination blood flow through these structures. Not all capillaries are active at the same time, and a single factor such as environmental temperature can have a dramatic effect on dermal perfusion. Additionally, tissue processing could significantly distort the cross-sectional area measured. Arterioles and capillaries in this investigation were oval to round, but venules varied from oval to flattened and occasionally indented. However, the correlation of the determined morphologic vascular parameters with established techniques using cutaneous vascular Doppler dosimetry could provide significant insight for predicting cutaneous blood flow. Montereiro-Riveire, *et al* (1990)[3] utilized Doppler dosimetry in their study but did not attempt to quantitate vascular features.

An unexpected finding from this investigation was that the hairless strains (Hairless Guinea pig, Fuzzy rat and SKH1 mouse) had higher fractional areas of follicles than the haired strains of the same species. Thus, the appearance of these genetically "hairless" mutants appears not to be due to the agenesis of hair. Also, the hairless strains had higher sebaceous gland fractional areas compared to the haired strains.

A second finding in this investigation was the observation that the surface follicular ostia often occurred in ordered rows. There was a similar distance between rows of ostia and between individual ostia within a row. This finding prompted the use of a non-routine section for surface follicular ostia counts per unit of surface area. This method allowed for visualization and enumeration of follicular ostia that were not possible from routine histologic sectioning.

The utility of methods used in this investigation allowed rapid collection of hundreds of measurements that would have been cost and time prohibitive without image analysis. The results of this investigation have brought to light the value of additional parameters to further define the anatomical characteristics between species. Such parameters include determining the dermis and subcutis depths and determining the correlation of vascular structures, especially capillary plexuses to adnexal elements. It also supports a recognition for the need of three-dimensional computer modeling and morphometry. A three dimensional model of skin coupled with an insight of cutaneous blood flow for any laboratory species could significantly aid in the advancement of dermal toxicology. This three-dimensional model would better define the relationship of adnexal structures to the superficial capillary plexus blood flow and the absorption of chemicals into the blood from the adnexa.

APPENDICES

Appendix A - Non-Standard Definitions

The following non-standard anatomical terms and definitions were applied to analyzed tissues:

- Viable epidermis - epidermal regions including the basal cell layer and extending to, but not including, the stratum granulosum
- Capillaries - vascular spaces lined by one or two visible endothelial cells
- Arterioles - vascular spaces lined by three or more endothelial cells surrounded by smooth muscle tunic
- Venules - vascular spaces lined by three or more endothelial cells and lack a smooth muscle tunic

Appendix B - Measurement Algorithms

This appendix contains a brief description of the computer-based algorithms used to measure the epidermis, vessels and adnexal structures in skin. A brief description of each step is included to avoid the complexity of proprietary computer code unique to the Quantimet 570c Image Analysis and to allow simplified vocabulary for those unaccustomed to image analysis terminology.

Skin, Epidermal Measurement Algorithm

1. Select image to measure and align tissue section for optimal presentation:
    A glass slide with processed and stained cutaneous tissue is placed on the microscope and aligned for proper orientation and tissue visibility for the CCD color camera. The surface of the skin is vertical and toward the left. The gain and offset are adjusted to properly illuminate the tissue.

2. Computer-based detection of background (viewed image without tissue):
    The tissue image is removed from the field of view, and the color and intensity of the clear glass slide are detected and stored in an image plane.

3. Convert analog image to digital image:
    The tissue is manually realigned to its previous position an analog image captured by the CCD camera is converted to a digital image by the video preprocessor. The digitized color image is stored in a 24-bit red-green-blue (RGB) format, with 8-bits being allocated for each color component.

4. Computer-based detection of granular cell layer:
    The granular layer stains a very dark blue due to the absorption of hematoxylin by the keratohyaline granules by the cells of this layer. The image analysis system identifies this blue color by thresholding on the digitized color image. The thresholding process entails specifying in each of the digitized color components a range of values which uniquely describe the color of the region of interest. The detected granular layer image is digitized in a video image plane, thus allowing for its position and size to be stored.

5. Computer-based detection of total epidermal area:
    The same tissue is manually realigned in the same position as when the granular layer was detected. The epidermis is stained shades of blue due to its affinity for hematoxylin, and the dermis is stained pink to red due to its affinity for eosin. The total epidermis is detected utilizing the difference in staining. Its size and location are stored in an image plane.

6. Computer-based determination of each area to be measured:
    The images stored in the three image planes will now be referred to as regions. They are:
    (a) region 1 = background
    (b) region 2 = total epidermis
    (c) region 3 = granular cell layer

21

Below are descriptions of the appropriate use of these regions. The position and size of the stratum corneum, stratum granulosum and the remaining viable epidermis can be recognized as distinct zones for measurement by using these descriptions accordingly. Once the zones have been determined, the width of the zone on a plane perpendicular to the surface is measured along a horizontal row of pixels, known as a chord. The zones can be identified by measuring from left to right as follows:

(1)   From the right edge of region 1 to the left edge of region 3 is the stratum corneum zone; in measuring, any space with the same color as the background is subtracted from the chord length.

(2)   Region 3 is the stratum granulosum zone.

(3)   From right edge of region 3 to right edge of region 2 is the remaining viable epidermis zone.

The width of each zone is measured by extrapolating the number of pixels on each chord and the calibrated width of a pixel at the magnification used to view the tissue. Multiple measurements are obtained by repeating the measurements every ten pixels on a vertical plane.

Skin, Dermal Vessel Measurement Algorithm

1.   Select image to measure:
A glass slide with the cutaneous tissue is placed on the microscope and aligned for proper orientation and tissue visibility for the CCD color camera. The surface of the skin is vertical and toward the left.

2.   Convert analog image to digital image:
The analog image captured by the CCD camera is converted to a digital image by the video preprocessor.

3.   Computer-based detection of the basement membrane:
The total epidermis is detected in the same manner as described in the epidermal measurement algorithm. Once detected, the right margin is identified to be the basement membrane.

4.   Apply computer-based grid overlay:
A basic problem of visualization and location of vessels is resolved by using a grid overlay. The features, such as capillaries, to be measured cannot be visualized at low magnification. When viewed at an adequately-increased magnification, the distance from the capillaries to the basement membrane is not within the field of view for all but the most superficial capillaries.

A computer generated grid is composed of parallel and perpendicular lines resulting in rows and columns of small boxes or grid cells. The application or overlay of a grid to a tissue section at low magnification allows for the precise determination of the bounding lines of the grid cell to an anatomical feature such as the basement membrane. The size

of each individual cell is the size of the field of view at high magnification. The computer generated grid is stored in a video image plane and used as a binary overlay.

When the individual grid cell is viewed at a (high) magnification to visualize capillaries, the image analysis system calculates the distance from the capillary to the grid cell border in the direction of the basement membrane and the distance from the grid cell border to the basement membrane. The sum of these two distances is the depth of the detected feature from the basement membrane.

5.   Select a grid element to be measured at higher magnification:
The measurement of the tissue involves manually selecting a grid cell, performing steps to measure features in that cell at a higher magnification, returning to low magnification and selecting the next grid cell until all cells have been evaluated.

6.   Alignment algorithm:
After a grid cell has been selected, the tissue associated with that cell must be aligned in the center of the field of view to allow for proper alignment at higher magnification. This is accomplished by the following steps:

(a)   Detect histologic features within a grid cell and convert them to image contours. The contours are stored in an image plane and will be used as a binary overlay for tissue alignment.

(b)   The image contour binary overlay from within the grid cell is positioned in the center of the field of view at low magnification. The tissue is then manually moved to align the features with the binary overlay.

(c)   Next, the binary overlay size is increased to equal that of the tissue at a higher magnification. The microscope objective is adjusted to the higher magnification, and the tissue is again manually aligned with the binary overlay. The tissue is now aligned to measure the desired features within the grid cell at high magnification.

7.   Computer-based detection of vessels:
Tissue sections used for vessel measurements are stained with H&E. The detection of endothelial-lined structures (vessels) was based on color thresholding.

8.   Vessel Measurements:
After the vessels are detected, they are manually defined by keyboard entry as either an arteriole, venule or capillary. The image analysis system measurement processor then performs the desired measurement of each individually detected feature, such as cross-sectional area. The depth of the vessel is determined in the manner described previously.

9.   Store Data:
The data obtained from measurements are stored in an ASCII file.

10. Return to low magnification and repeat for each subsequent grid segment until the measurement of grid cells is complete.

<u>Dermal Adnexal Measurement Algorithm</u>
The procedure used for adnexal measurements is similar to that used for vascular measurements but differs in two ways. Masson's trichrome is used to stain the tissues resulting in different detectable colors for connective tissue, hairs and follicular epithelium/glandular epithelium. The second difference is that hair follicles and sebaceous glands are the measured features.

<u>Skin, Dermal Follicular Count</u> (follicle to surface area)

1. Select image to measure:
   The second tissue specimen was sectioned to allow for determination of the number of follicular ostia per cutaneous surface (see Materials and Methods - Sample Preparation). A glass slide with the cutaneous tissue is placed on the microscope (20x magnification) and aligned for proper orientation and tissue visibility for the CCD camera.

2. Convert analog image to digital image:
   The analog image captured by the CCD camera is converted to a digital image by the video preprocessor.

3. Manually count follicular ostia in field of view:
   The follicular ostia in each examined section are counted and tabulated manually.

CITATIONS

1. Nailbach, P.E., Dermatotoxicology; *in* - Principles and Methods of Toxicology, A.W. Hayes Editor, 2nd Edition, Raven Press, New York, 1989, p.383-406.

2. All, N., Oehme, F.W., A Literature Review of Dermatotoxicity
Vet Hum Toxicol 34-5:428-437, 1992.

3. Monteiro-Riviere, N., Bristol, D.G., Manning T.O., Rogers, J.A. and Riviere, J.E., Interspecies and interregional analysis of the comparative histologic thickness and laser Doppler blood flow measurement of five cutaneous sites in nine species. J. Invest. Dermatol 95:582-586, 1990.

GENERAL REFERENCES

Morphology
DeHoff R.T. and Hines, F.N. 1967. Quantitative Microscopy. McGraw-Hill, New York, NY

Weibel, E.R. 1979. Stereological Methods, Vol. 1. Practical Methods for Biological Morphometry. Academic Press, Inc., New York, NY.

Weibel, E.R. 1979. Stereological Methods, Vol. 2. Theoretical Foundations. Academic Press, Inc., New York, NY.

Basic Cutaneous Anatomy
Weiss, L., ed. 1983. Histology, Cell and Tissue Biology, 5th Edition. Elsvier Scientific Co. Inc., New York, NY.

Dellman, H-D. and Brown E.M. 1976. Textbook of Veterinary Histology. Lea & Febiger, Philadelphia, PA

Fowler, E.H. and Calhound, M.L. 1964. The microscopic anatomy of developing fetal pig skin Am. J. Vet Res., 25:156.

Montaga, W. 1962. The Structure and Function of Skin Academic Press, Inc., New York, NY.

Rothmanns, S. 1954. Physiology and Biochemistry of the Skin The University of Chicago Press, Chicago, IL.

Langman, J. 1981. Medical Embryology, 4th Edition. The Williams & Wilkins Company, Baltimore, MD.

Metabolism
Goldsmith, L.A. 1983. Biochemistry and Physiology of Skin Oxford University Press, Oxford, England.

Claude, P. 1978. Morphological factors influencing transepithelial permeability: A model for the resistance of the zonula occludens J. Membrane Biol. 39:219.

Schneeberger, E. 1978. Structural basis for some permeability of the air-blood barrier Fed. Proc 37:2471.

Kefalides, N.A., Alper, R., and Clarke, C.C. 1979. Biochemistry and metabolism of basement membranes. Int. Rev. Cytol. 61:167.

Basic Dermal Toxicology
Drill, V.A., and Lazar, P. 1987. Cutaneous Toxicity. Academic Press, Inc., New York, NY.

V.A. Drill, ed. 1980. Current Concepts in Cutaneous Toxicity Academic Press, Inc., San Diego, CA.

Ritschel, W.A., and Hussain, A.S. 1988. The principles of permeation of substances across the skin. Meth. Find. Exptl. Clin. Pharmacol. 10: 39-56.

Kronevi, T., Wahlberg, J., and Holmberg, B. 1979. Histopathology of skin, liver, and kidney after epicutaneous administration of five industrial solvents to guinea pigs. Environ. Res. 19, 56-69.

Epidermis and Keratinization
Dale, B.A., Holbrook, K.A., and Steinert. P.M. 1978. Assembly of stratum corneum, basic protein and keratin filament in microfibrils. Nature (London) 276:729.

Elias, P.M. and Friend, D.S. 1975. The permeability barrier in the mammalian epidermis. J. Cell Biol. 276: 180.

Elias, P.M. McNutt, N.S. and Friend, D.S. 1977. Membrane alterations during cornification of mammalian squamous epithelia: A freeze-fracture, tracer and thin section study. Anat. Rec. 189:577.

Dermal-Epidermal Junction
Briggaman, R.A. 1982. Biochemical composition of the epidermal-dermal junction and other basement membranes. J. Invest. Dermatol. 78:1.

Dermis
Goldsmith, L.A. 1983. Biochemistry and Physiology of Skin. Oxford University Press, Oxford, England.

Marzuli, F.N., and Maibach, H.I. 1987. Dermatotoxicology, 3rd edition. Hemphisphere, Washington D.C.

Collagen
Bornstein, P., and Raub, W. 1979. The Chemistry and Biology of Collagen In The Proteins. Vol 4, Neurath, H. and Hill, R.L. (eds.), Academic Press, Inc., New York, NY.

Adipocyte
Greenwood, M.R.C., and Hirsch, J. 1974. Postnatal development of adipocyte cellularity in the normal rat. J. Cell Biol. 15:474.